Supplementary materials

Structure-function analysis of time-resolved immunological phases in metabolic dysfunction-associated fatty liver disease.

Anja Schmidt-Christensen[1], Gustaw Eriksson[2], William Michael Laprade[3] and Behnaz Pirzamanbein[3,4], Maria Hörnberg[5], Kajsa Linde[5], Julia Nilsson[1,5], Mark Skarsfeldt[6], Diana Julie Leeming[6], Rajmund Mokso[7], Mariana Verezhak[8], Anders Dahl[4], Vedrana Dahl[4], Kristina Önnerhag[9], Massoud Rezaee Oghazi[10], Sofia Mayans[5] and Dan Holmberg[1,5,11]

[1]Lund University Diabetes Center, Lund University, Lund Sweden; [2]Karolinska Institute, Stockholm, Sweden; [3]Technical University of Denmark, DTU; [4]Statistics department, Lund University, Lund Sweden; [5]Inficure Bio AB, Umeå Sweden; [6]Nordic Bioscience A/S, Herlev, Denmark; [7]MAXIV laboratory, [8]Paul Scherrer Institut, Villigen, Switzerland; [9]Skåne hospital, Malmö, Sweden; [10]Connected Pathology, Belgium; [11]Department of Medical Biosciences, Umeå University, Umeå Sweden;

Contents:

	Page
Supplementary methods	01
Bioinformatics data analysis	02
Processing of SRμCT data.	03
Suppl. Fig. 1	04
Suppl. Fig. 2	06
Suppl. Fig. 3	07
Suppl. Fig. 4	08
Suppl. Fig. 5	10
Suppl. Table 1a DEGs control mice 3 vs. 6 w	Excell file
Suppl. Table 1b DEGs control mice 6 vs. 18 w	Excell file
Suppl. Table 1c DEGs control mice 3 vs. 18 w	Excell file
Suppl. Table 2a DEGs NIF mice 3 vs. 6 w	Excell file
Suppl. Table 2b DEGs NIF mice 6 vs. 18 w	Excell file
Suppl. Table 2c DEGs NIF mice 3 vs. 18 w	Excell file
Suppl. Table 3a DEGs NIF mice 3 vs. 6 w age corrected	Excell file
Suppl. Table 3b DEGs NIF mice 6 vs. 18 w age corrected	Excell file
Suppl. Table 3c DEGs NIF mice 3 vs. 18 w age corrected	Excell file
Suppl. Table 4a GEO analysis of genes found in Table S3a.	Excell file
Suppl. Table 4b GEO analysis of genes found in Table S3a.	Excell file
Suppl. Table 4c GEO analysis of genes found in Table S3a.	Excell file
Suppl. Table 5 Animal models used for comparative analysis	12
Supplementary videos 1-3	mov. files

Bioinformatics data analysis

Differential gene expression utilized DESeq2 (20) with four contrasts used for comparing differential expression (controls week 3 vs. controls week 6, controls week 6 vs. controls week 18, NIF week 3 vs. NIF week 6, NIF week 6 vs. NIF week 18) using the DESeq2 default Wald's test. DEG's were identified by Benjamini-Hochberg (BH) (21) adjusted p-value <0.05 and log2 fold change (log2FC) ≥1. The data was transformed using variance stabilizing transformations (Suppl. Fig. 2) and non-coding genes were excluded before downstream visualization with heatmaps and gene set enrichment analysis. GSEA was performed using the clusterProfiler package (22) and enrichGO for biological processes on two sets of DEG's per comparison, denoted as either upregulated or downregulated based on a positive or negative log2FC. GO's containing ≥3 DEG's and BH adjusted p-value <0.05 were determined to be significant and enriched. Molecular pathway dysregulation in the liver tissues was determined by Gene Set Enrichment Analysis (GSEA) surveying molecular pathways gene sets in Molecular Signature Database (MSigDB) (www.broadinstitute.org/msigdb) (Suppl. Table 1). Cross-species comparison was performed in the space of molecular pathway gene sets from Hallmark and KEGG databases (https://www.gsea-msigdb.org/ gsea/msigdb/genesets.jsp) as specified in Suppl. Fig. 4 and Suppl. Table 2, and similarity to the human datasets was determined by Euclidean distance and visualized as previously described by Tsuchida et al. (23).

The significance values (p-value of overlap) for the IPA canonical pathways were calculated by the right-tailed Fisher's Exact Test, and the p-values were adjusted for multiple testing using BH (24). It was also required that at least two DEGs were associated with an enriched pathway. A ratio was calculated of the number of DEG molecules associated with a given pathway divided by the total number of molecules in the reference set that map to the pathway.

IPA also calculated for each pathway a z-score that predicted pathway activation if positive or inhibition if negative. The z-score was calculated by comparing the dataset fold changes under analysis with the canonical pathway patterns in the IPA Knowledge Base. Z-scores of ≥ _2 or ≤ _-2 are considered significant, and no z-score annotation indicates either zero (or very close to zero) z-score or that the given pathway is ineligible for a prediction.

The IPA Molecule Activity Prediction (MAP) tool was used for making predictions of the activation or inhibition statuses of interacting molecules. Diagrams were extended by adding connections to the ten most significantly associated diseases and functions or the ten most significantly associated liver-related functions.

Processing of synchrotron radiation-based microtomography (SRμCT) data.

Each of the 36 specimens had two to three randomly selected regions scanned. Using monochromatic photons (21 keV), transmitted X-ray photons were converted into visible light via a 20-μm LuAG:Ce scintillator screen, coupled to a sCMOS detector (2160x2560 pixels) with 1.6μm (4x) and 325 nm (20x) effective pixel sizes. Paganin et al.´s algorithm (13) was employed for phase retrieval. Volumes at 20x magnification were cropped to 1600 x 1600 x 1600 and downscaled to 800 x 800 x 800 via 2x binning for computational efficiency without accuracy loss. Linear model correction addressed bias fields, masked intensity reduction minimized bright artifacts, and volume intensities were normalized.

Suppl. Fig. 1

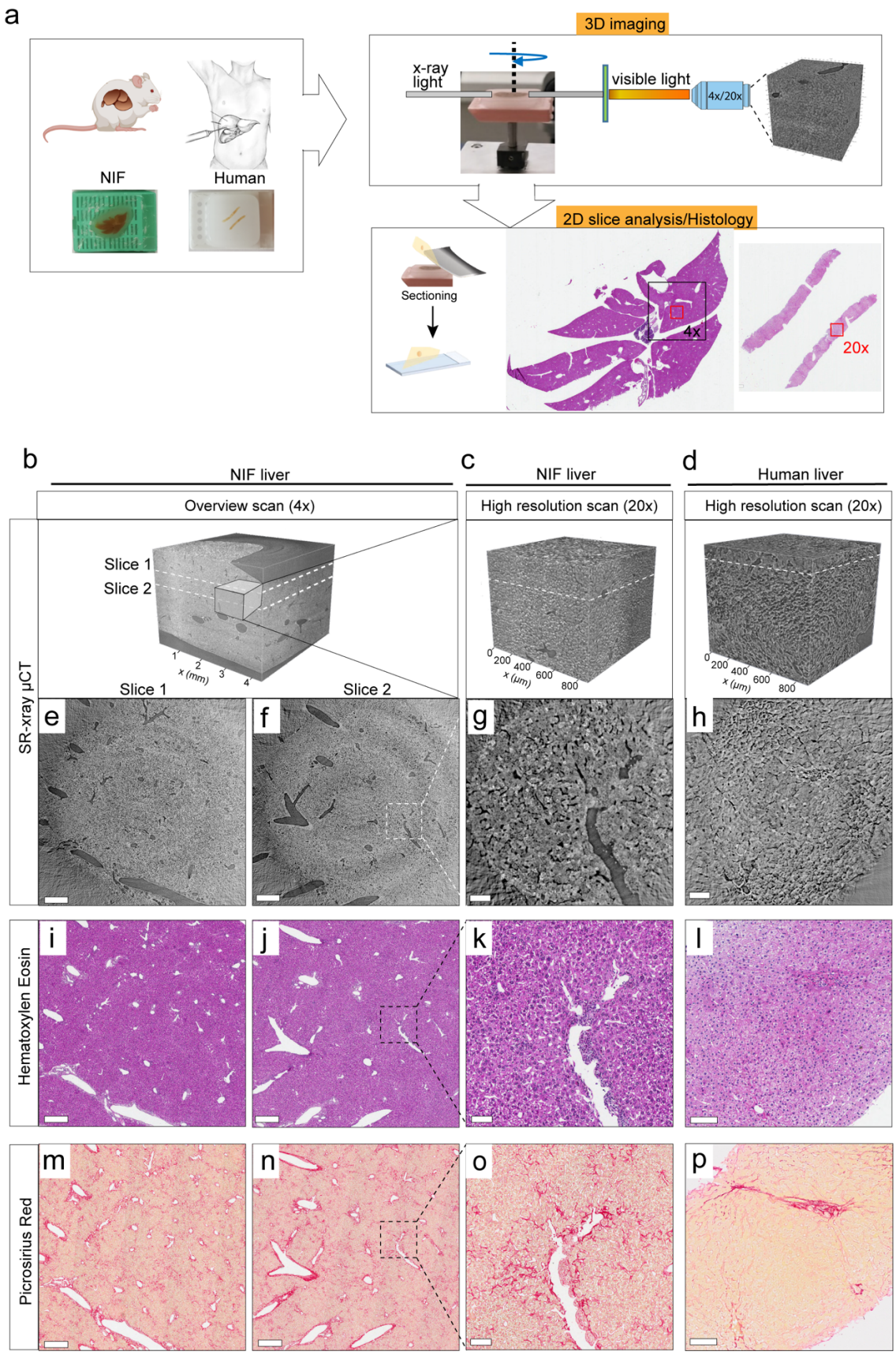
a
3D imaging
x-ray light
visible light
4x/20x
NIF
Human
2D slice analysis/Histology
Sectioning
4x
20x
b
NIF liver
Overview scan (4x)
c
NIF liver
High resolution scan (20x)
d
Human liver
High resolution scan (20x)
SR-xray µCT
Slice 1
Slice 2
x (mm)
x (µm)
e
f
g
h
Hematoxylen Eosin
i
j
k
l
Picrosirius Red
m
n
o
p

Suppl. Fig. 1: SR-µCT enables virtual histology for human biopsies and larger animal tissues. (a) Experimental setup for the structural tomographic SR-x-ray µCT imaging of fixed human liver biopsies and mouse liver samples followed by sectioning of the liver tissue blocks and conventional 2D histology for validation. Field of view for overview or high-resolution SR-x-ray µCT is indicated by black or red square for 4x or 20x magnification respectively. (b-h) Liver samples obtained from 12-week old NIF mice (b,c, e-g) or human healthy volunteers (d,h) were subjected to overview (b,e,f) and/or high-resolution SR-µCT imaging (c,d,g,h). 3D-renderings (b-d) or 2D cross-sections (e-h), as indicated in b-d, matched with corresponding histological sections stained with Hematoxylen and Eosin (i-l) or Picrosirius Red (m-p). Scale bar: 500 µm (e,f,i,j,m,n) or 100µm (g,h,k,l,o,p).

Suppl. Fig. 2

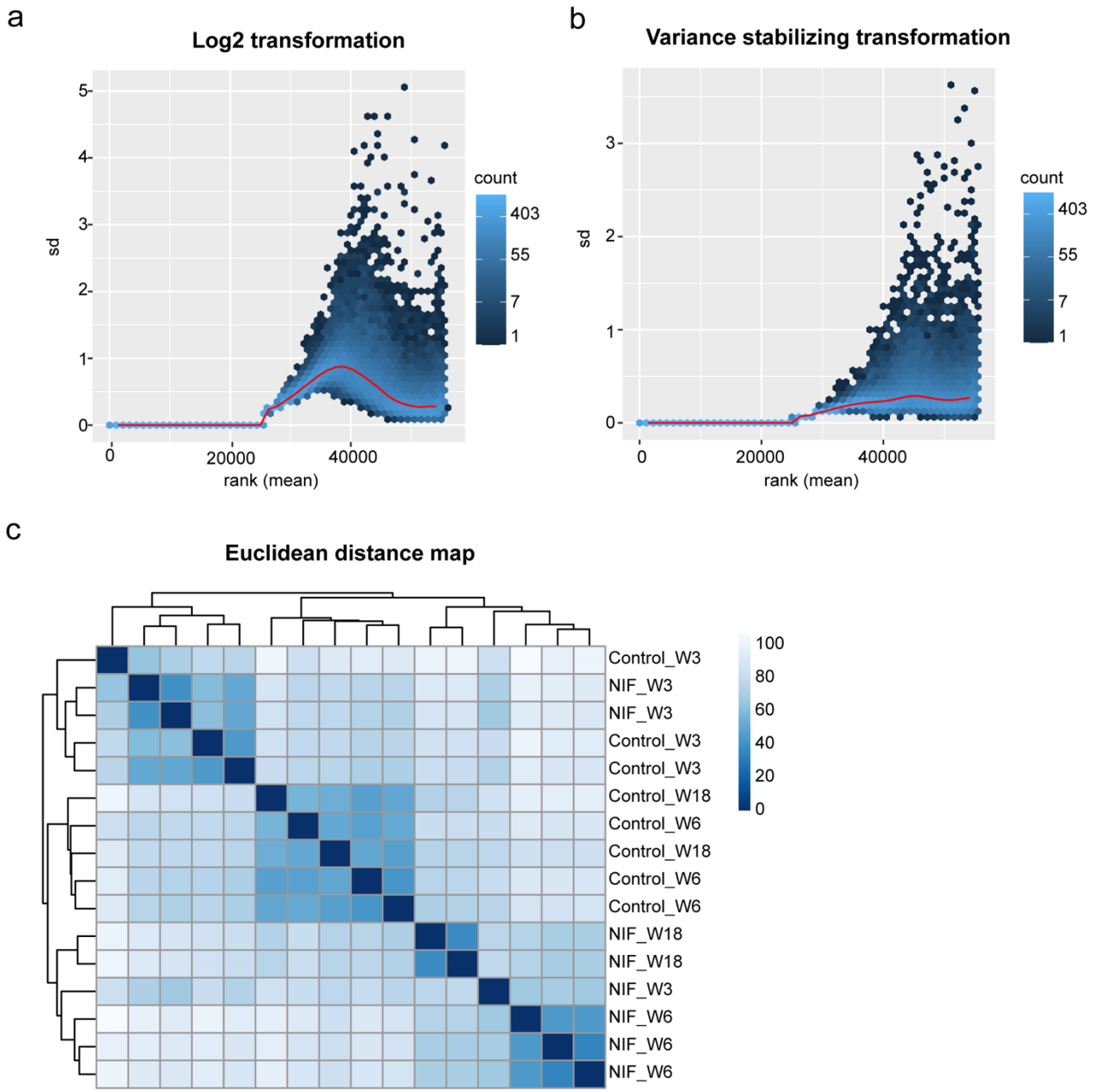

Suppl. Fig. 2: The standard deviation (sd) and ranked mean are calculated from the gene expression matrix row-wise per gene across all column-wise samples, to generate the scatterplot (a-b) after log2 normalization (a) and variance stabilizing transformation (b). The red line in (a-b) indicates the running median estimator of the gene expression matrix and the scale bar and dot color indicate the mean count. Euclidean distances between gene expression matrices with hierarchical clustering are presented in (c) to present similarity between the samples shown in the scale bar where 0 is similar and 100 is dissimilar Euclidean distance.

Suppl. Fig. 3

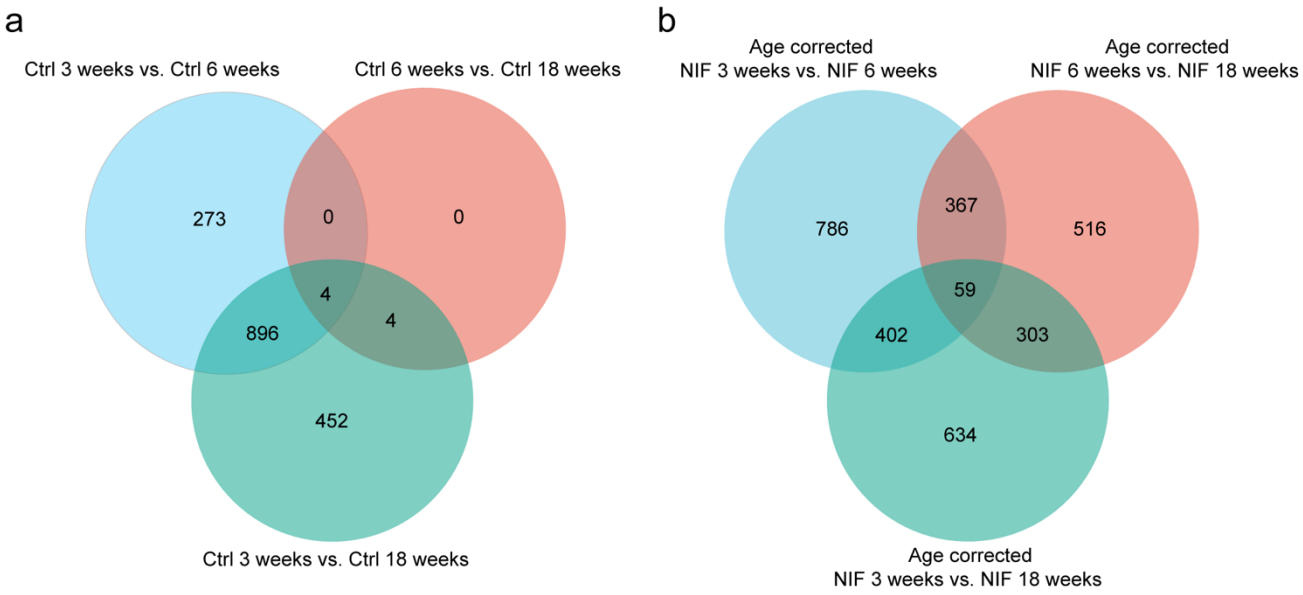

Suppl. Fig. 3: Venn diagrams indicating shared and unique differentially expressed genes (DEG) in liver transcriptomes across ages of 24αβNOD control (a) and NIF mice corrected for age related DEGs (b), that have been identified in (a). Timepoints were strategically selected to capture disease progression (related to Fig.4), including pre-disease onset at 3 weeks, early-stage phenotype at 6 weeks and late-stage.

Suppl. Fig. 4.

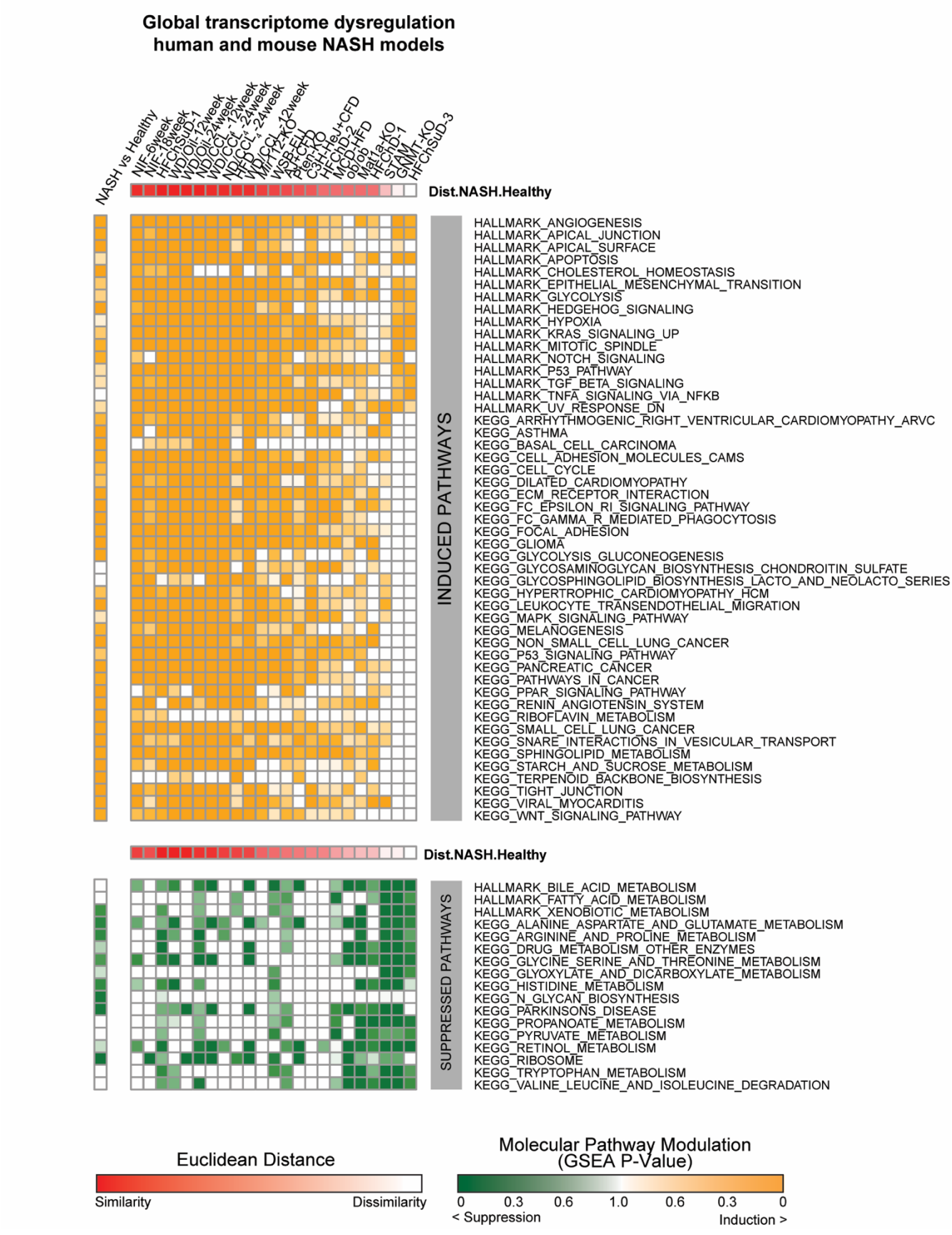
Global transcriptome dysregulation
human and mouse NASH models
NASH vs Healthy
NIF-6week
NIF-18week
HFChSuD-1
WDOil-12week
WDOil-24week
NDCCl4-12week
WDCCl4-24week
NDCCl4-24week
WDCCl4-12week
MUP-uPA
WSB-EH
Pten-KO
C3H-HeJ+CFD
HFChD-2
MCD-HFD
ob/ob
Mat1a-KO
HFChD-1
STAM
GNMT-KO
HFChSuD-3
Dist.NASH.Healthy
INDUCED PATHWAYS
HALLMARK_ANGIOGENESIS
HALLMARK_APICAL_JUNCTION
HALLMARK_APICAL_SURFACE
HALLMARK_APOPTOSIS
HALLMARK_CHOLESTEROL_HOMEOSTASIS
HALLMARK_EPITHELIAL_MESENCHYMAL_TRANSITION
HALLMARK_GLYCOLYSIS
HALLMARK_HEDGEHOG_SIGNALING
HALLMARK_HYPOXIA
HALLMARK_KRAS_SIGNALING_UP
HALLMARK_MITOTIC_SPINDLE
HALLMARK_NOTCH_SIGNALING
HALLMARK_P53_PATHWAY
HALLMARK_TGF_BETA_SIGNALING
HALLMARK_TNFA_SIGNALING_VIA_NFKB
HALLMARK_UV_RESPONSE_DN
KEGG_ARRHYTHMOGENIC_RIGHT_VENTRICULAR_CARDIOMYOPATHY_ARVC
KEGG_ASTHMA
KEGG_BASAL_CELL_CARCINOMA
KEGG_CELL_ADHESION_MOLECULES_CAMS
KEGG_CELL_CYCLE
KEGG_DILATED_CARDIOMYOPATHY
KEGG_ECM_RECEPTOR_INTERACTION
KEGG_FC_EPSILON_RI_SIGNALING_PATHWAY
KEGG_FC_GAMMA_R_MEDIATED_PHAGOCYTOSIS
KEGG_FOCAL_ADHESION
KEGG_GLIOMA
KEGG_GLYCOLYSIS_GLUCONEOGENESIS
KEGG_GLYCOSAMINOGLYCAN_BIOSYNTHESIS_CHONDROITIN_SULFATE
KEGG_GLYCOSPHINGOLIPID_BIOSYNTHESIS_LACTO_AND_NEOLACTO_SERIES
KEGG_HYPERTROPHIC_CARDIOMYOPATHY_HCM
KEGG_LEUKOCYTE_TRANSENDOTHELIAL_MIGRATION
KEGG_MAPK_SIGNALING_PATHWAY
KEGG_MELANOGENESIS
KEGG_NON_SMALL_CELL_LUNG_CANCER
KEGG_P53_SIGNALING_PATHWAY
KEGG_PANCREATIC_CANCER
KEGG_PATHWAYS_IN_CANCER
KEGG_PPAR_SIGNALING_PATHWAY
KEGG_RENIN_ANGIOTENSIN_SYSTEM
KEGG_RIBOFLAVIN_METABOLISM
KEGG_SMALL_CELL_LUNG_CANCER
KEGG_SNARE_INTERACTIONS_IN_VESICULAR_TRANSPORT
KEGG_SPHINGOLIPID_METABOLISM
KEGG_STARCH_AND_SUCROSE_METABOLISM
KEGG_TERPENOID_BACKBONE_BIOSYNTHESIS
KEGG_TIGHT_JUNCTION
KEGG_VIRAL_MYOCARDITIS
KEGG_WNT_SIGNALING_PATHWAY
Dist.NASH.Healthy
SUPPRESSED PATHWAYS
HALLMARK_BILE_ACID_METABOLISM
HALLMARK_FATTY_ACID_METABOLISM
HALLMARK_XENOBIOTIC_METABOLISM
KEGG_ALANINE_ASPARTATE_AND_GLUTAMATE_METABOLISM
KEGG_ARGININE_AND_PROLINE_METABOLISM
KEGG_DRUG_METABOLISM_OTHER_ENZYMES
KEGG_GLYCINE_SERINE_AND_THREONINE_METABOLISM
KEGG_GLYOXYLATE_AND_DICARBOXYLATE_METABOLISM
KEGG_HISTIDINE_METABOLISM
KEGG_N_GLYCAN_BIOSYNTHESIS
KEGG_PARKINSONS_DISEASE
KEGG_PROPANOATE_METABOLISM
KEGG_PYRUVATE_METABOLISM
KEGG_RETINOL_METABOLISM
KEGG_RIBOSOME
KEGG_TRYPTOPHAN_METABOLISM
KEGG_VALINE_LEUCINE_AND_ISOLEUCINE_DEGRADATION
Euclidean Distance
Similarity
Dissimilarity
Molecular Pathway Modulation
(GSEA P-Value)
0
0.3
0.6
1.0
0.6
0.3
0
< Suppression
Induction >

Suppl. Fig. 4: Comparative hepatic gene expression in NIF mice, human NASH-associated gene and other mouse models for NASH. Heat map of cross-species sample Similarity of human NASH liver transcriptome datasets (NASH patients vs. healthy individuals) vs. NIF 6 weeks, NIF 18 weeks and a panel of 16 previously published diet, chemical, and/or genetic NASH mouse models (26) with statistically significant dysregulation defined as FDR <0.01 in either of the two human MASH liver transcriptome datasets: advanced vs. mild NAFLD (MASLD) patients (GSE49541), and NASH (MASH) patients vs. healthy individuals (GSE48452). Dysregulation of the selected gene sets was similarly determined by GSEA in a panel of 16 previously published diet, chemical, and/or genetic MASH mouse models (Suppl. Table 1), Dysregulation of the selected gene sets was determined by GSEA and similarity to the human datasets was determined by Euclidean distance. Red color on heat map indicates FDR values for the transcriptome similarity. Top ranked induced (orange) or suppressed (green).

Suppl. Fig. 5

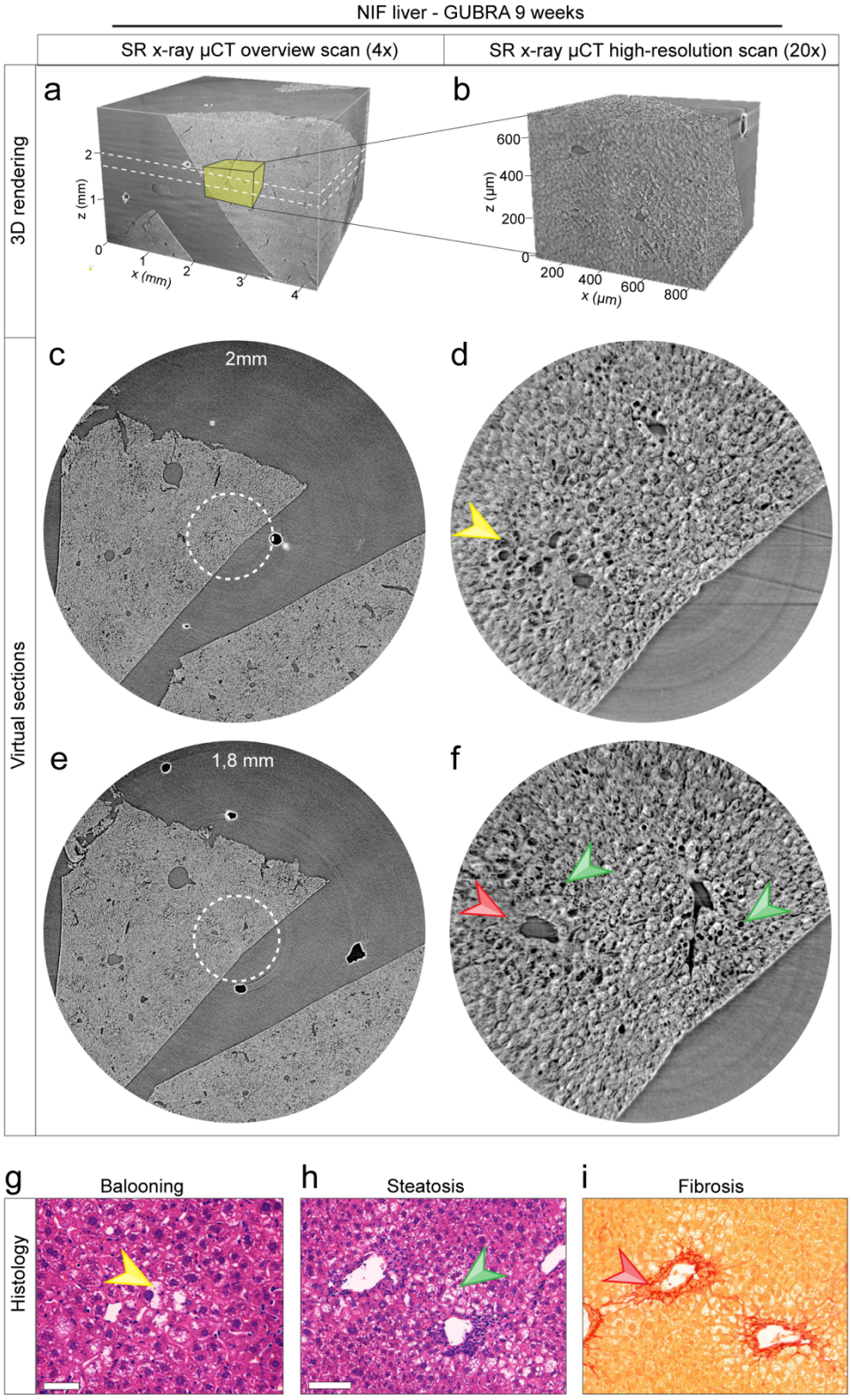
NIF liver - GUBRA 9 weeks
SR x-ray µCT overview scan (4x)
SR x-ray µCT high-resolution scan (20x)
3D rendering
Virtual sections
a
b
c
d
e
f
2mm
1,8 mm
z (mm)
x (mm)
z (µm)
x (µm)
g
h
i
Balooning
Steatosis
Fibrosis
Histology

Suppl. Fig. 5: SR-µCT imaging reveals characteristics of NASH in GAN diet fed NIF mice. Liver samples obtained from 12-week-old NIF mice that have been fed GAN diet for 9 weeks were subjected to both overview (a, c, e) and high-resolution SR-µCT imaging (b, d, f). 3D-renderings (a, b) or 2D cross-sections (c-f) and Field-of-view for the corresponding high-resolution scan as indicated in (a, c, e). (g-i) Corresponding histological sections stained with Hematoxylin and Eosin (g, h) or Picrosirius Red (i). Notable structures and features are labelled: fat cell denoted by green arrow (f, h), ballooning hepatocyte by yellow arrow (d, g) and fibrosis by red arrow (d, i). Scale bar 100µm (g-i).

Suppl. Table 5 GSEA comparison mouse models

GSE Acession number	Tissue	Model
48452	Liver (human)	NASH / CTRL
49541	Liver (human)	Advanced / Mild NAFLD
22608	Liver (mouse)	OB / WT
27713	Liver (mouse)	KO / WT
35961	Liver (mouse)	NASH Metformin / Normal
38013	Liver (mouse)	SHPKO West Diet / Chow
38141	Liver (mouse)	West Diet / Control Diet
39594	Liver (mouse)	High fat / Normal
59042	Liver (mouse)	High fat / Normal
62362(a)	Liver (mouse)	WSB-CFD 12Week / CTRL
62362 (b)	Liver (mouse)	AJ-CFG 12Week / CTRL
62362 (c)	Liver (mouse)	C3H-CFD 12Week / CTRL
63027 (a)	Liver (mouse)	*gnmt* KO / WT
63027 (b)	Liver (mouse)	*mat1a* KO / WT
67680	Liver (mouse)	West Diet / Control Diet
70681	Liver (mouse)	Mutant / WT
83596	Liver (mouse)	Tumour / Non-Tumour
99010 (a)	Liver (mouse)	WDCCL4 12Week / CTRL
99010 (b)	Liver (mouse)	WDOil 12Week / CTRL
99010 (c)	Liver (mouse)	WDOil 24Week / CTRL
99010 (d)	Liver (mouse)	WDCCL4 24Week / CTRL
99010 (e)	Liver (mouse)	NDCCL4 12Week / CTRL
99010 (f)	Liver (mouse)	NDCCL4 24Week / CTRL